p-Cresol Methylhydroxylase: Alteration of the Structure of the Flavoprotein Subunit upon Its Binding to the Cytochrome Subunit[†,‡]

Louise M. Cunane,[§] Zhi-wei Chen,[§] William S. McIntire,[||] and F. Scott Mathews*[,§]

Department of Biochemistry and Molecular Biophysics, Washington University School of Medicine, St. Louis, Missouri 63110, Molecular Biology Division, Department of Veterans Affairs Medical Center, San Francisco, California 94121, and Department of Biochemistry and Biophysics, University of California, San Francisco, California 94143

Received September 14, 2004; Revised Manuscript Received November 30, 2004

ABSTRACT: The structures of two forms of a recombinant flavoprotein have been determined at high resolution and compared. These proteins are (1) the flavocytochrome *c p*-cresol methylhydroxylase (rPCMH, 1.85 Å resolution) and (2) the cytochrome-free flavoprotein subunit of rPCMH (PchF, 1.30 Å resolution). A significant conformational difference is observed in a protein segment that is in contact with the *re* face of the isoalloxazine ring of FAD when the structure of PchF is compared to the subunit in the intact flavocytochrome. This structural change is important for optimum catalytic function of the flavoprotein, which has been shown to be dependent on the presence of the cytochrome subunit. This change results in different protein−flavin and apparently different protein−substrate interactions that have a "tuning effect" on the electronic and redox properties of bound *p*-cresol and the covalently bound FAD. The conformational change in the segment in the cofactor-binding site is induced by a small rearrangement in the flavoprotein−cytochrome interface region of the flavoprotein.

The degradation of the toxic phenol *p*-cresol by Pseudomonads occurs by way of the protocatechuate metabolic pathway (*1*). The first enzyme in this pathway, *p*-cresol methylhydroxylase (PCMH,[1] EC 1.17.99.1), a flavocytochrome *c*, catalyzes the oxidation of *p*-cresol to *p*-hydroxybenzyl alcohol (Figure 1). During catalysis, a quinone methide intermediate is formed by removal of two electrons and two protons from *p*-cresol. These electrons are captured by the flavin prosthetic group, yielding one molecule of fully reduced FAD (*2*). The electrons are then passed one at a time from FAD to the heme cofactor by intramolecular electron transfer and subsequently to cytochrome oxidase within the periplasmic membrane via soluble electron carrier proteins; the protons are lost to bulk solvent. Hydroxylation of the quinone methide intermediate is believed to occur by nucleophilic attack by water at the methide carbon to yield *p*-hydroxybenzyl alcohol (Figure 1). PCMH is able also to oxidize this alcohol to *p*-hydroxybenzaldehyde, which is then oxidized to *p*-hydroxybenzoic acid by the second enzyme in the protocatechuate pathway, *p*-hydroxybenzaldehyde dehydrogenase (*3*).

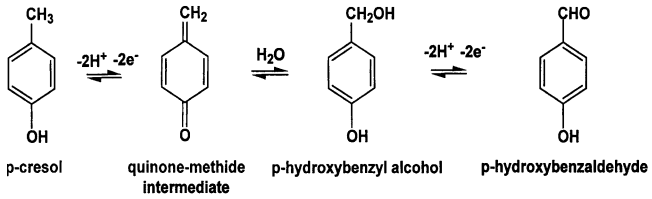

FIGURE 1: Reactions catalyzed by *p*-cresol methylhydroxylase (PCMH). The product of the first reaction, *p*-hydroxybenzyl alcohol, can serve as substrate for a second reaction to produce *p*-hydroxybenzaldehyde.

PCMH is an $\alpha_2\beta_2$ heterotetramer with an M_r of 136 000 (Figure 2) that can be resolved by isoelectric focusing into two components which differ by ~0.5 unit in pI (*4*, *5*). The holoenzyme $(\alpha_2\beta_2)^2$ can be reconstituted from the separated components with full restoration of enzymatic function. One component is a monomeric *c*-type cytochrome (β or PchC) with an M_r of 9200 (*6*), and the other is an α_2 flavoprotein homodimer ($PchF_2$) with an M_r of $2 \times 58\,700$ (*3*). PchF contains FAD bound covalently ($PchF^C$) through the 8-methyl position of its isoalloxazine ring to a tyrosine side chain (*7*). The X-ray crystal structure of PCMH from *Pseudomonas*

[†] This work was supported by NIH Grant GM-20530 and NSF Grant MCB-0091084 (F.S.M.), by a Department of Veterans Affairs Merit Review Grant, and by NIH Grant GM-061651 (W.S.M.). Use of the Advanced Photon Source was supported by the U.S. Department of Energy, Basic Energy Sciences, Office of Science, under Contract W-31-109-Eng-38.

[‡] Crystallographic coordinates for the recombinant PCMH heterotetramer and the $PchF^C$ flavoprotein homodimer have been deposited in the Protein Data Bank as entries 1WVE and 1WVF, respectively.

* To whom correspondence should be addressed: Department of Biochemistry and Molecular Biophysics, Washington University School of Medicine, St. Louis, MO 63110. E-mail: mathews@biochem.wustl.edu. Phone: (314) 362-1080. Fax: (314) 362-7183.

[§] Washington University School of Medicine.

[||] Department of Veterans Affairs Medical Center and University of California.

[1] Abbreviations: HPLC, high-performance liquid chromatography; NCS, noncrystallographic symmetry; PCMH, *p*-cresol methylhydroxylase; PCMH[Y384F], PCMH containing Y384F-flavoprotein subunits; PchC, β *c*-type cytochrome subunit of PCMH; PchF, α flavoprotein subunit of PCMH with covalently bound FAD, unless otherwise noted; $PchF^C$ and $PchF^{NC}$, PchF harboring covalently and noncovalently bound FAD, respectively; $PchF_2^C$, actual dimeric form of $PchF^C$; PchF[Y384F], Y384F mutant form of PchF; PES, phenazine ethosulfate; rPCMH, recombinant *p*-cresol methylhydroxylase; rmsd, root-mean-square deviation.

[2] The β symbol refers to a residue in the cytochrome subunit.

10.1021/bi048020r CCC: $30.25
Published on Web 02/03/2005

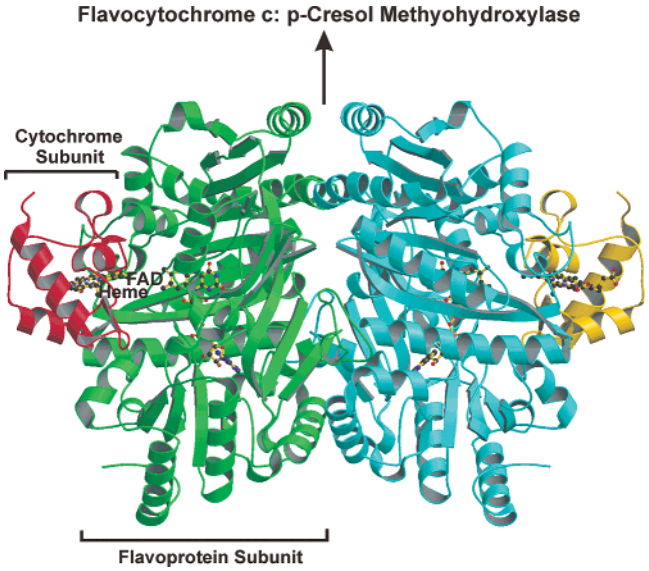

FIGURE 2: rPCMH heterotetramer, showing the flavoprotein dimer and the cytochrome subunits flanking it on either side. The locations of cofactors FAD and HEME are also indicated. A molecular 2-fold axis (represented by an arrow) runs vertically through the flavoprotein dimer interface, in the plane of the paper. This figure was prepared using MOLSCRIPT (*28*) and rendered with RASTER3D (*29*).

putida was determined previously in this laboratory (*8*), with and without a bound substrate, at 2.75 and 2.5 Å resolution, respectively. The major difference in their structures, besides the presence of a ligand at the active site, was the concerted movement of several side chains that serve to regulate access from bulk solvent to the active site. The proposed reaction mechanism was supported by the observed structural features, including the putative "gated" entry or exit portal for substrate and product to or from the buried active site, and a possible means of ferrying out protons produced in the reaction. The flavoprotein subunit (as the α_2 dimer containing noncovalently bound FAD), the cytochrome subunit, and the intact $\alpha_2\beta_2$ flavocytochrome have all been overexpressed in recombinant form in *Escherichia coli* (*9*).

The biochemical properties of the separated flavoprotein and cytochrome components differ markedly from those of the intact flavocytochrome. The isolated flavoprotein dimer, harboring covalently bound FAD, has less than 1% of the catalytic activity toward *p*-cresol of the flavocytochrome (*10*), although the K_m values for the artificial electron acceptor phenazine methosulfate and for *p*-cresol are relatively unchanged (*5*, *11*). The one-electron redox potential of the isolated cytochrome subunit (157 mV) is lower by ~80−90 mV than that in the native complex (234−249 mV); the two-electron redox potential of the cytochrome-free PchF subunit is ~20−30 mV lower (60−65 mV) than that in the native complex (85−93 mV) (*12*, *13*).

Of considerable interest is the reason for covalent tethering of FAD in PCMH and other flavoproteins. Approximately 10% of known flavoproteins have FAD or FMN covalently bound to protein, in one of five binding modes, and the mechanism of formation and the purpose are under active investigation (*14*). It has been shown that FAD tightly bound noncovalently to PchF ($PchF^{NC}$) will not undergo covalent attachment to this subunit unless PchC is also present (*15*); i.e., the flavinylation process is only self-catalytic in the PCMH complex. A mechanism for this process has been proposed (*15*). Interestingly, the covalent link is not required for preventing the loss of FAD (*16*). However, catalytic activity with *p*-cresol is extremely slow under anaerobic conditions when FAD is noncovalently bound to cytochrome-free PchF, although slow oxidation of *p*-hydroxybenzyl alcohol can be observed (*16*). It was discovered also that the electronic properties of *p*-cresol are very different when it is bound to PCMH as opposed to dimeric $PchF_2^C$; the two-electron redox potential for the substrate is ~380 mV lower in PCMH than in $PchF^C$, which, in large part, explains the dramatic difference in the activities for these two proteins (*9*).

For PCMH, it has been deduced that the covalent linkage serves several purposes. (a) It is responsible for a significant increase in the two-electron redox potential of covalently bound FAD in $PchF^C$ (62 mV) relative to this subunit with noncovalently bound FAD (−16 mV), which (*10*, *17*, *18*), in part, explains the significantly higher activity of the former protein. (b) The covalent bond is a component of major electron transfer conduits from the flavin to the heme (*8*, *15*). (c) A comparison of $PCMH[Y384F]^{NC}$, in which the FAD attachment site is absent, and normal PCMH indicates that the covalent tethering is essential for the extremely tight association of the $PchF^C$−PchC complex which results in the difference in the potential of the heme of ~50 mV (186 mV for $PCMH[Y384F]^{NC}$ and 234−249 mV for normal PCMH) (*13*).

It was found that the potentials of the heme (186 mV) and FAD (47 mV) in $PCMH[Y384F]^{NC}$ are greater than those of free PchC (157 mV) and free $PchF[Y384F]^{NC}$ (2 mV), respectively. Therefore, even with noncovalently bound FAD, subunit association causes significant changes in the environments of the two prosthetic groups.

In this paper, we describe the crystal structure of recombinant PCMH (rPCMH) at an improved resolution of 1.85 Å, and the crystal structure of $PchF_2^C$ at 1.30 Å resolution. Conformational changes are described for the flavoprotein that occur within the $PchF^C$−PchC interface and within a pair of polypeptide segments of $PchF^C$ comprising 16 residues that are packed against the *re* face of the flavin ring when the two subunit types come together to form the flavocytochrome complex.

MATERIALS AND METHODS

As described elsewhere, rPCMH was purified from *E. coli* strain DH5α transformed with the pKK vector harboring both *pchF* and *pchC* (*9*). The intact rPCMH, with covalently bound FAD, was subjected to preparative isoelectric focusing in a flat bed of Sephadex G-200 Superfine using Pharmalyte 4.5−6 ampholytes (Amersham Biosciences). This procedure separates completely the flavoprotein dimer (pI 5.0) from the monomeric cytochrome subunit (pI 4.5) (*5*, *10*, *19*). Bands containing $PchF^C$ and PchC were scraped off the flat bed separately, diluted with buffer, and eluted from the Sephadex in small columns. Ampholytes were removed from the protein solutions, and the buffer was replaced with five or six concentration/dilution cycles using Centircon-30 ($PchF^C$) or Centricon-10 (PchC) centrifuge concentrators (Amicon).

Crystals of both rPCMH and $PchF^C$ were grown by the sitting drop vapor diffusion method (*20*). For rPCMH, 5 μL

Table 1: Data Collection and Refinement Statistics for Recombinant *p*-Cresol Methylhydroxylase (rPCMH) and the Separate Flavoprotein Subunit ($PchF^C$)

	rPCMH	$PchF^C$
data collection		
wavelength (Å)	1.5418	0.9000
space group	$P2_12_12_1$	$C2$
a (Å)	73.83	88.64
b (Å)	118.60	116.91
c (Å)	136.21	50.22
β (deg)	(90)	113.20
asymmetric unit	heterotetramer ($\alpha_2\beta_2$)	monomer (α)
maximum resolution (outer shell) (Å)	1.85 (1.92−1.85)	1.30 (1.35−1.30)
$I/\sigma(I)$[a]	18.6 (2.1)	19.6 (4.1)
no. of observations	466728	428736
no. unique reflections	94080	100440
% completion (outer shell)	90.9 (52.3)	87.3 (46.1)
redundancy	5.1 (1.5)	4.3 (2.1)
R_{merge}[b] (outer shell)	0.067 (0.285)	0.089 (0.155)
refinement		
data range (Å)	30−1.85	30−1.30
no. of reflections	94068	100433
R_{work}[c]	0.159	0.146
R_{free}[c]	0.194	0.167
test set fraction (%)	10	10
rmsd for bond lengths (Å)	0.010	0.011
rmsd for bond angles (deg)	1.52	1.63
$\langle B\rangle$ for protein atoms (Å^2)	21.8	11.0
$\langle B\rangle$ for solvent atoms (Å^2)	33.6	27.1
rms ΔB (m/m, Å^2)[d]	1.18	0.86
rms ΔB (m/s, Å^2)[d]	1.45	1.23
rms ΔB (s/s, Å^2)[d]	2.23	2.07
Ramachandran plot[e]		
most favored (%)	90.6	91.8
additionally allowed (%)	8.8	8.0
generously allowed (%)	0.4	0.2
disallowed (%)	0.2	0.0

[a] $I/\sigma(I)$ is the average signal-to-noise ratio for merged reflection intensities. [b] $R_{merge} = \sum_h\sum_i|I(h) - I_i(h)|/\sum_h\sum_i I_i(h)$, where $I_i(h)$ is the ith measurement and $I(h)$ values are the mean measurements of reflection h. [c] $R = \sum_h|F_o - F_c|/\sum_h|F_o|$, where F_o and F_c are the observed and calculated structure factor amplitudes, respectively, of reflection h. R_{free} is the R for the test reflection data set for cross validation of the refinement (*24*), and R_{work} is the R for the working reflection set. [d] Root-mean-square difference in the *B*-factor for bonded atoms; m/m, m/c, and c/c represent main chain−main chain, main chain−side chain, and side chain−side chain bonds, respectively. [e] Calculated using PROCHECK (*27*).

of protein solution at 10 mg/mL in 10 mM Tris buffer (pH 8.5) was mixed with an equal volume of a reservoir solution containing 11−14% PEG 8000, 200 mM ammonium acetate, and 100 mM Tris buffer (pH 8.5) and left to equilibrate at 23 °C. Crystals reached dimensions of approximately 0.5 mm × 0.4 mm × 0.25 mm in ~2 weeks. For the $PchF^C$, 5 μL of protein solution at 10 mg/mL in 10 mM acetate buffer (pH 4.5) and 5 μL of reservoir solution containing 25% PEG 1500, 200 mM magnesium acetate, and 50 mM acetate buffer (pH 4.5) were mixed and allowed to equilibrate at 23 °C. Single crystals grew to an approximate size of 0.6 mm × 0.5 mm × 0.25 mm in 1−2 weeks.

X-ray diffraction data were collected from rPCMH on an R-axis IV image plate system mounted on a Rikagu RU-200 rotating anode X-ray generator operating at 50 kV and 100 mA. Data for the $PchF^C$ were collected on beamline 19ID of the Structural Biology Center at the Advanced Photon Source (Argonne National Laboratory, Argonne, IL). In the latter case, a two-pass data set to 1.3 Å resolution was collected. In both cases, crystals were flash frozen in a stream of liquid nitrogen at −170 °C, and the data were processed with the HKL package (*21*). For cryoprotection, the rPCMH crystal was coated with Paratone oil; for $PchF^C$, the crystal was soaked for 3 min in a solution containing 32% PEG 1500, 200 mM magnesium acetate, 50 mM acetate buffer (pH 4.5), and 25% glycerol. The data collection statistics are presented in Table 1.

The structure of $PchF^C$ was determined by molecular replacement using AMoRe (*22*) with the flavoprotein component of the earlier structure of PCMH determined at room temperature at 2.5 Å resolution (*8*) used as a search molecule. The crystals of rPCMH are approximately isomorphous to those of the native crystals, but a reduction in cell dimensions at low temperatures warranted solution by molecular replacement, which was also accomplished with AMoRe, again using the earlier room-temperature structure of PCMH as the search model. Both structures were refined using CNS (*23*) employing similar strategies for refinement. Ten percent of the reflections were chosen randomly to form a test set for cross validation (*24*). An initial round of rigid-body refinement at 2.5 Å resolution was carried out for both models followed by positional, simulated annealing, and temperature factor refinement. The resolution of both models was gradually extended to the recorded limit, and the two models were manually rebuilt using Turbo-Frodo (*25*). A few additional rounds of minimization, including bulk solvent correction, simulated annealing, *B*-factor refinement, and model rebuilding, were each followed by the gradual interactive addition of water molecules. For rPCMH, non-crystallographic symmetry (NCS) restraints were applied to the model. At the final stage of refinement, a number of residues having alternate conformations were included in both structures. For rPCMH to 1.85 Å resolution, the final $R_{work} = 0.159$ and $R_{free} = 0.193$, with rmsds from ideal values of 0.010 Å for bond lengths and 1.52° for bond angles. For $PchF^C$ refined to 1.30 Å resolution, R_{work} and R_{free} equaled 0.146 and 0.167, respectively, with rmsds of 0.11 Å and 1.63° for bond lengths and bond angles, respectively. The refinement statistics for both molecules are summarized in Table 1.

RESULTS

Structure Analysis. rPCMH crystallizes in orthorhombic space group $P2_12_12_1$ and contains one $\alpha_2\beta_2$ heterotetramer in the asymmetric unit (for cell dimensions, see Table 1). The flavoprotein α-chain extends from residue 7 to 521 in both subunits, the first six residues being absent from the electron density; the cytochrome β-chain is visible from position 2 to 76 with the first and last four residues absent. In both subunits, the extent of the visible α-subunit is the same as in the earlier 2.5 Å resolution structure (*8*), whereas the β-subunit extends two residues beyond that in the previously determined structure. The final model for rPCMH consists of 1180 amino acid residues, 4 acetate ions, 2 chloride ions, 4 Tris ions, and 1103 water molecules. A total of 18 residues in the two flavoprotein subunits of rPMCH were found to exist in two alternate conformations of approximately equal occupancy, 7 in one and 11 in the other, with 3 of these common to both subunits.

$PchF_2^C$ crystallizes in monoclinic space group $C2$ and contains one α-subunit in the asymmetric unit. The dimeric

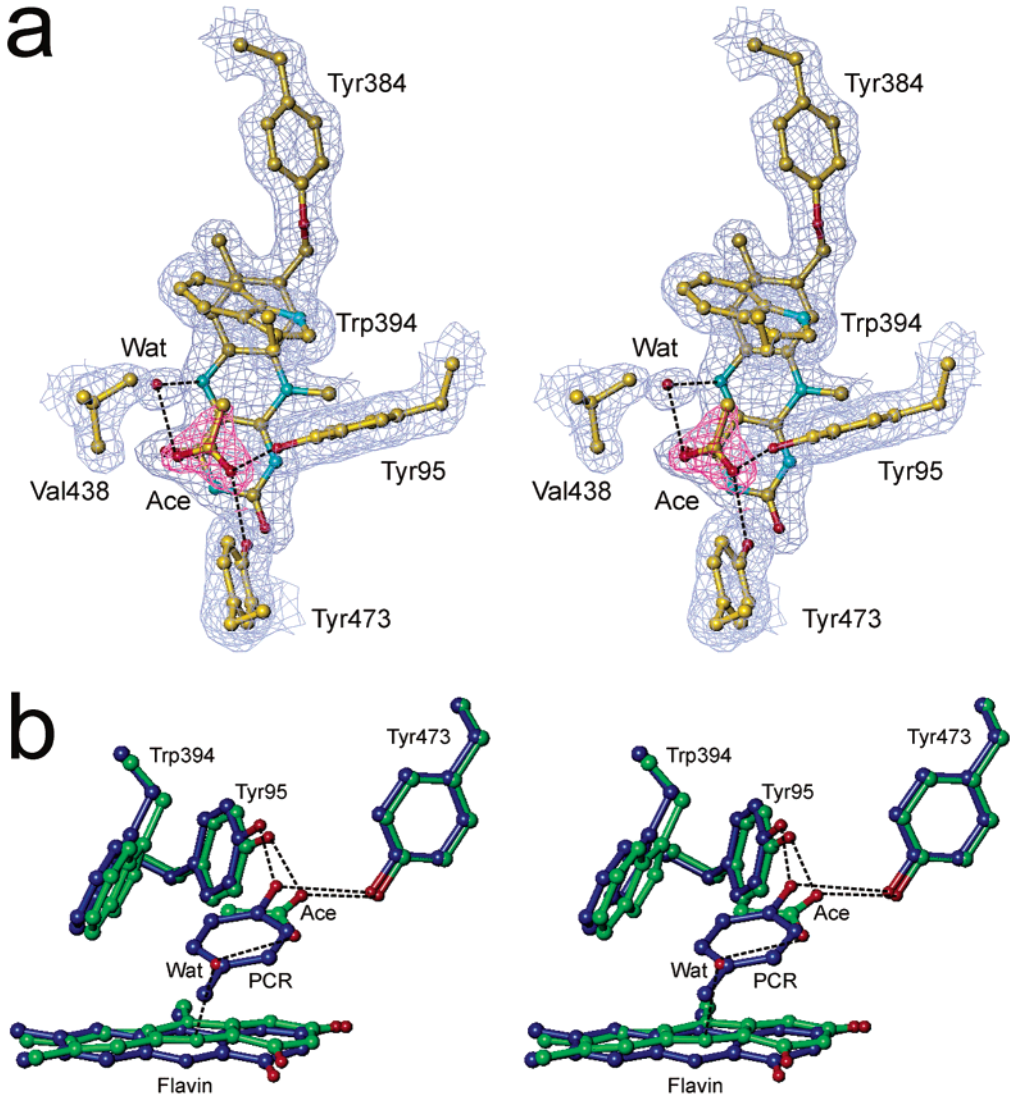

FIGURE 3: Active site of one of the α-subunits of rPCMH. (a) Electron density showing the flavin ring and an acetate anion bound in the active site. The side chain of Tyr384 that is covalently attached to the C8M position is also shown, as are the side chains of Tyr95 and Tyr473 and a water that binds to the oxygen atoms of the acetate. Also shown are the side chains of Trp394 and Val438 that help provide a hydrophobic environment for the methyl group of the acetate. The electron density is contoured at the 1σ level. (b) Comparison of the active sites of rPCMH (green) and the *p*-cresol complex of PCMH determined previously (*8*) (blue) showing the relative orientations of the bound acetate and *p*-cresol molecules. Oxygen atoms are colored red. The water molecule bridging one of the oxygen atoms of the acetate and the flavin N5 atom is also shown. This figure was prepared using TURBO-FRODO (*30*).

arrangement of the two α-subunits of $PchF_2^C$ in the crystal is identical to that in rPCMH (Figure 2), and the 2-fold axis of symmetry of $PchF_2^C$ is coincident with one of the crystallographic 2-fold axes of the unit cell. The final model for the $PchF^C$ subunit consists of 515 amino acid residues, 2 acetate ions, 1 chloride ion, 2 glycerol molecules, and 801 water molecules. Twenty-two of the residues are in two alternate conformations in the molecule, and one exists in three alternate conformations. These results, along with an analysis of the Ramachandran plots (*26*) of the two proteins, are presented in Table 1.

Comparison of rPCMH with Native Structures. The rPCMH structure reported here binds four molecules of acetate ion per molecule, two at apparently adventitious, nonfunctional surface sites and one within each of the two actives sites of the α_2 flavoprotein, close to each of the flavin rings (Figure 3a). The binding of the acetate molecule mimics that of *p*-cresol within the PCMH−*p*-cresol complex determined earlier at 2.75 Å resolution [Protein Data Bank (PDB) entry 1DIQ] (*8*) (Figure 3b). The acetate is approximately coplanar with *p*-cresol, ~4 Å above the flavin ring, and forms hydrogen bonds between one of its oxygen atoms and the hydroxyl groups of Tyr95 and Tyr473, as does the hydroxyl of the substrate. The other oxygen is bridged to N5 of flavin by a water molecule (Figure 3a). The acetate methyl group is surrounded by hydrophobic interactions with Val438, Trp394, and C10 of the flavin ring at distances of 3.6−3.7 Å. When the structure of the α-subunit of rPCMH is compared with those of the free and substrate-bound forms of native PCMH, the rmsds for all 515 equivalent Cα atoms are 0.423 and 0.293 Å, respectively. Some of the side chain positions that are characteristic of PCMH in the *p*-cresol-bound form in which the active site is in a closed form are also found in rPCMH such as those of Tyr473 and His436 and of one of the two alternate conformers of Glu177 which forms a hydrogen bond to His436 (*8*). In addition, a tripeptide (Phe152-Ser153-Ala154) close to the *re* face of the flavin ring that differs in conformation between the free and

Table 2: Hydrogen Bonding between the Flavoprotein and Cytochrome Subunits of rPCMH

flavoprotein subunit	cytochrome subunit	type of interaction	distance (Å)
Lys46 N^{ζ}	Arg48 O	side−main	2.70[a]
Arg91 $N^{\eta 1}$	Ala52 O	side−main	2.76[a]
Asp109 $O^{\delta 1}$	Ser56 O^{γ}	side−side	2.60[a]
Asp139 $O^{\delta 1}$	Lys13 N^{ζ}	side−main	2.96[a]
Ile158 O	Tyr57 O^{η}	main−side	2.67[a]
His291 $N^{\delta 1}$	Val23 O	side−main	2.93[a]
Asn385 $N^{\delta 2}$	Val25 O	side−main	2.85[a]
Gln40 O	Ala55 N	water bridge	2.99[b]
Val42 O	Asn45 O	water bridge	2.76[b]
Tyr44 O^{η}	Ser56 N	water bridge	2.88[b]
Lys111 N^{ζ}	Ser56 O	water bridge	2.96[b]
Leu378 N	His17 O	water bridge	2.79[b]
Gln379 $O^{\epsilon 1}$	Glu22 O	water bridge	2.84[b]
Gly389 N	heme $O^{\delta 2}$	water bridge	2.92[b]

[a] Average hydrogen bonding distance between the two pairs of subunits. [b] Average of four bridging hydrogen bonding distances over the two pairs of subunits.

substrate-bound forms of native PCMH (rmsd = 0.99 Å for the three Cα atoms) is much closer in conformation in rPCMH to the substrate-bound form (0.35 Å rmsd) than to the free form (0.78 Å rmsd) of the native enzyme.

The interface between the flavoprotein and cytochrome subunits in rPCMH is virtually the same as in the free and substrate-bound native enzyme (*8*). In those structures, the buried interface is ∼1100 Å^2 per subunit, and the residue composition is ∼50% hydrophobic and 30% neutral hydrophilic. The minimum flavin−heme separation in rPCMH (7.3 Å) is slightly shorter than the values reported previously for the substrate-free and substrate-bound forms of PCMH (7.6 and 7.7 Å, respectively), while the flavin N5−heme iron distance in rPCMH (18.0 Å) is approximately midway between the values in these same forms of PCMH (18.5 and 17.7 Å, respectively). The seven hydrogen bonds observed previously that connect the flavoprotein and cytochrome subunits, six of which involve side chains of the flavoprotein subunit, are retained. In addition, there are seven bridging water molecules not previously described; both sets of hydrogen bonds are conserved in the two pairs of $\alpha\beta$ subunits (Table 2).

Comparison of the Lone Flavoprotein Dimer with the Flavocytochrome. In $PchF_2^C$, one acetate anion is bound in the substrate-binding site on the *si* face of the flavin ring, as it is in rPCMH (Figure 4). The only difference is in the water bridge connecting the acetate to N5 of the flavin, which involves two waters for $PchF^C$ instead of one. The configuration of several key groups also resembles that of the "closed-gate" form of the PCMH (*8*). Thus, the presence of acetate in the active site appears to lead both rPCMH and $PchF^C$ to adopt a substrate-bound type of conformation. The flavin ring of $PchF^C$ is also oriented in a manner similar to that of rPCMH and the native *p*-cresol complex, differing to a greater extent (by ∼15° in tilt angle) from that of the native free form of PCMH. However, the side chain of Tyr384 of isolated $PchF_2^C$ that serves as a covalent link to the flavin ring from the enzyme exists in two alternate conformations that differ by ∼45° in the orientation of the phenyl ring (Figure 4).

Conformational Changes in $PchF^C$ that Occur upon Binding of the Cytochrome Subunit. $PchF^C$ exhibits an rmsd of 0.377 Å for 515 equivalent Cα positions with respect to rPCMH. In contrast, the rmsd between all 590 matched residues of the two pairs of $\alpha\beta$ subunits of rPCMH is 0.066 Å. When the $PchF^C$ and rPCMH flavoprotein structures are examined in detail, several significant conformational differences are found between the subunit in the absence and presence of the cytochrome. These differences are localized to 14 separate amino acid segments ranging from one to eight residues in length (Table 3). These differences are of three types. One is "packing", where the segments are localized to the protein surface but are not within the flavoprotein−cytochrome interface, and the dissimilarities are caused by differences in crystal packing in the two crystallographic unit cells. Another is "local", where the conformational change is localized to the cytochrome−flavoprotein interface and is induced either by hydrogen bond formation or by close van der Waals contacts between the subunits. The third is "coupled" and is also induced by the formation of hydrogen bonds or by close contacts with PchC, but involves conformational changes that propagate to the flavoprotein interior from the interface or are involved in a cooperative interaction with another such segment. Five of the differences are packing, seven are local, and two are coupled. The conformational changes attributed to packing are probably functionally unimportant and will not be further discussed.

When $PchF^C$ binds to PchC, formation of the six hydrogen bonds from its side chain atoms to atoms of the cytochrome (Table 2) leads to the seven local conformational changes in this subunit that occur upon complex formation (Table 3 and Figure 5). These local changes are small, with an average rmsd of 0.35 Å, and their segments are short, ranging from one to three residues in length. In five of these cases (2, 3, and 5−7, Table 3), the $PchF^C$ residue whose side chain is directly involved in the hydrogen bond is contained within the local segment that undergoes structural change; in the remaining two cases (1 and 4), the residue involved in the hydrogen bond is nearby. These six side chain hydrogen bonds from the flavoprotein subunit to the cytochrome appear to play a role primarily in stabilizing the complex and to be additive, that is, to act independently of one another. One possible exception may be the last residue, Asn385, in the seventh local segment, which may play a dual role. This segment contains Tyr384, which forms the covalent bond to the C8M atom of the flavin ring. After formation of the $PchF^C$−PchC complex, the aromatic ring of this tyrosyl residue becomes locked into a single conformation instead of existing in two discrete conformations as are found in the uncomplexed $PchF^C$ structure (Figure 4). As for the cytochrome subunit, unfortunately, nothing is known about any comparable distortions upon binding to the flavoprotein since the structure of uncomplexed PchC is not known.

The two coupled conformational changes in $PchF^C$ (Table 3) are considerably larger in magnitude than the local type, with an average rmsd of 1.4 Å, and are more extensive, each involving eight residues; they also appear to involve concerted movements of both segments. Both segments are generally located centrally in the interface (Figure 5), although the segment of residues 374−381 extends to the edge of the interface. The segment of residues 374−381 lies on the flavoprotein surface in an extended form with all of its residues partially exposed to solvent in the absence of the cytochrome subunit. The other segment, residues 152−

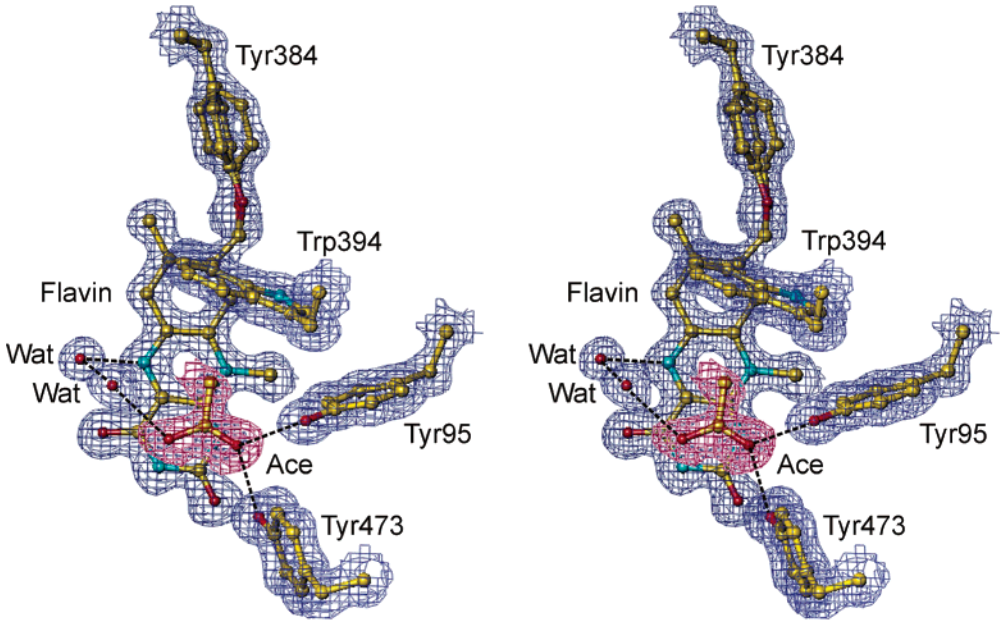

FIGURE 4: Electron density showing the flavin ring and the bound acetate anion in the active site of PchF^C. The side chains of Trp394, along with those of Tyr95 and Tyr473 and two water molecules that connect them to the acetate, are also shown. The two conformations exhibited by the side chain of Tyr384 covalently bound to the flavin can be visualized in the electron density. The orientation of the diagram is similar to that of Figure 3a, and the electron density is contoured at the 1σ level. This figure was prepared using TURBO-FRODO (*30*).

Table 3: Segments in Cytochrome-Free PchF^C Structure that Differ Significantly in Main Chain and/or Side Chain Conformation from the Cytochrome-Associated Domain of rPCMH

peptide segment	rmsd for Cα atoms (Å)	type	cause
Gly12-Val13	0.91	packing	differences in crystal contacts
Tyr140−Asn144	0.83	packing	differences in crystal contacts
Thr299−Pro301	0.55	packing	differences in crystal contacts
Pro305−Ser307	0.67	packing	differences in crystal contacts
Gln356−Gln363	0.70	packing	differences in crystal contacts
Leu41−Pro43	0.58	local (1)	close interaction with the cytochrome subunit
Lys46	0.38	local (2)	Lys46 side chain forms hydrogen bond to cytochrome
Arg91	0.06	local (3)	Arg91 side chain moves to form hydrogen bond with cytochrome
Lys111	0.39	local (4)	Lys111 moves when Asp109 forms H-bond with Ser56 of cytochrome subunit
Asp139	0.44	local (5)	Asp139 forms ion pair with cytochrome
Ala290−Leu292	0.50	local (6)	His291 side chain moves to form H-bond to cytochrome
Tyr384-Asn385	0.42	local (7)	Asn385 forms side chain−main chain hydrogen bond to cytochrome; Tyr384 has two alternate conformations in PchF^C but not in rPCMH
Phe152−Ala159	1.96	coupled	Ile158 carbonyl oxygen interacts with the cytochrome, forming H-bond to side chain
Gly374−Phe381	0.82	coupled	Leu378 makes close contact with cytochrome side chain and Phe381 makes close contact to heme vinyl methylene group of cytochrome

159, protrudes largely into the flavoprotein interior, with only two of its eight residues (157 and 158) exposed to solvent in the absence of the cytochrome.

The largest structural change in the segment of residues 374−381, when PchF^C binds to PchC to form PCMH, occurs at the side chains of Leu378 and Phe381 which are forced to move 1.5 and 2.7 Å away from PchC, respectively, as the two subunits push against each other (Figure 5b). Despite these large side chain movements, the backbone movement is less than 1 Å and all main and side chain hydrogen bonds to water or nearby protein atoms from Leu378 to Phe381 are maintained except for those to two water molecules, one of which is blocked by the cytochrome in rPCMH (Figure 6). At the other end of the segment, Gly374 also maintains all of its main chain hydrogen bond interactions. The greatest change in the hydrogen bonding pattern occurs for residues Val375−Asn377, although much of the pattern is still maintained. Here, the large structural alteration results from the net loss of three main chain hydrogen bonds with nearby protein atoms that occur in rPCMH but not in PchF^C, particularly with residues Ala154 and Ser156 from the other coupled segment.

The most striking difference (1.96 Å rmsd over eight residues) occurs in the main chain and side chain conformations of the segment comprising residues 152−159, which abuts the *re* face of the flavin ring (Figure 6). This change is much larger than that which was observed previously in residues 152−154 of this segment (0.99 Å rmsd over three residues) on the binding of *p*-cresol to PCMH (*8*). Concomitant with the concerted movement of the segment of residues 374−381 upon cytochrome binding, the side chain of Ile158 moves 2.8−4.5 Å toward the flavin's isoalloxazine ring and the main chain moves 1.0−1.5 Å to allow formation of the seventh interprotein hydrogen bond, between the main chain

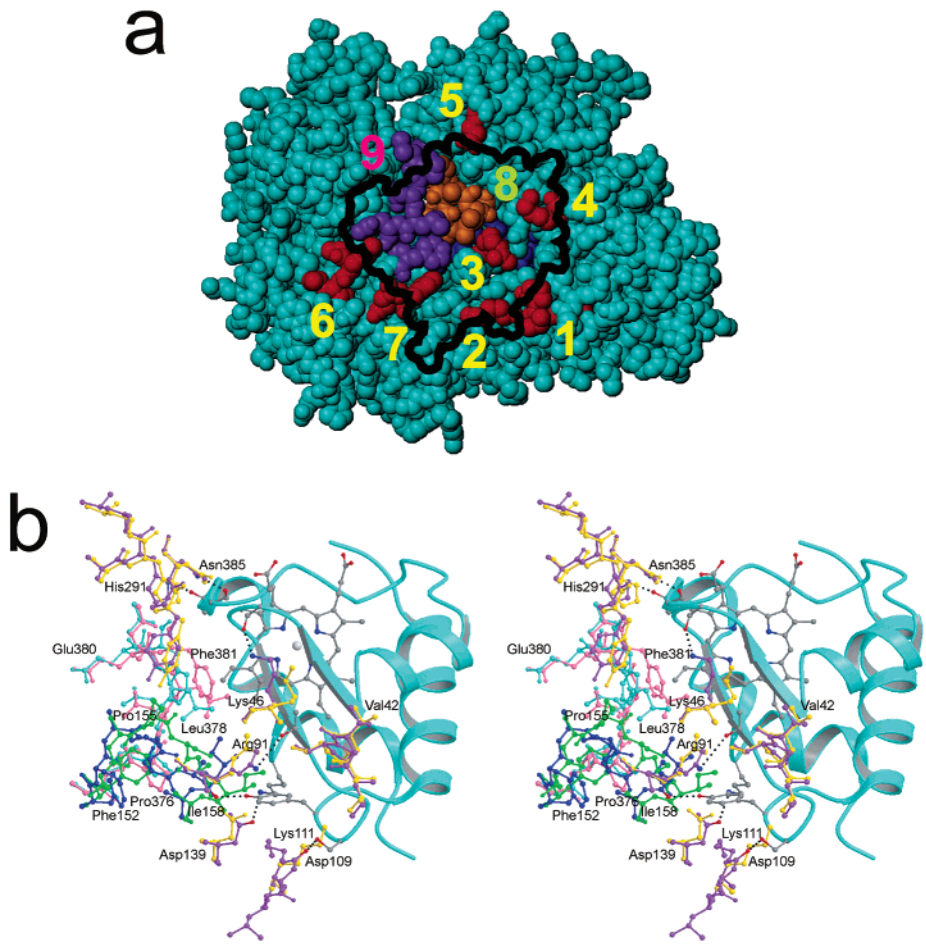

FIGURE 5: Nine segments of the flavoprotein subunit that exhibit significant local and coupled conformational changes (Table 3) upon binding to the cytochrome subunit. (a) Space filling model of the flavoprotein of PCMH with the seven local segments colored red, and numbered 1−7 in yellow, and the two coupled segments of residues 152−159 (gold) and 374−381 (violet) numbered 8 and 9 in green and magenta, respectively. A trace of the cytochrome subunit that shields part of the flavoprotein subunit is colored black. This panel was prepared using TURBO-FRODO (*30*). (b) Ribbon model of the cytochrome subunit of rPCMH and the segments of its flavoprotein subunit and of PchF^{C} that show conformational changes shown as balls and sticks. The cytochrome ribbon is colored cyan, and the heme and selected side cytochrome atoms are shown in atom colors (carbon in dark gray, nitrogen in blue, oxygen in red, and iron in light gray). The seven interacting local segments of the flavoprotein subunit of rPCMH are colored violet, and those of PchF^{C} are colored gold, except for nitrogens (blue) and oxygens (red) that are involved in hydrogen bonds. The segment of residues 152−159 of rPCMH and of PchF^{C} are colored dark blue and green, respectively, while those of residues 374−381 are colored cyan and pink, respectively. All seven hydrogen bonds that are formed in the PCMH complex are shown as dotted lines. The positions of selected residues are indicated. This panel was prepared using MOLSCRIPT (*28*) and rendered with RASTER3D (*29*).

carbonyl oxygen of Ile158 of the flavoprotein subunit and βTyr57^{2} O$^{\eta}$ of the cytochrome (Table 2 and Figures 5b and 7). These main chain and side chain movements impinge drastically upon the remainder of the polypeptide from Phe152 to Ala157, resulting in a dramatic change in the backbone conformation and side chain orientation of Phe152−Ser156 (Figures 6 and 7). These concerted changes lead to a major reorganization of the environment of the *re* face of the flavin ring opposite the *si* face active site cavity. In PchF^{C}, the *re* face is covered by residues Ser153, Ala143, and Pro155, with the proline ring approximately parallel to the dimethylbenzene ring of the flavin. In the rPCMH flavoprotein subunit, Ser153 still covers the pyrimidine ring, Ala154 is farther away, and the plane of Pro155 is nearly perpendicular to the flavin ring, lying above the C5a−C9a bond. Phe381 also comes closer to the flavin ring in rPCMH (Figure 6) and is now located above the C7M and C8M methyl groups.

The structural change in the segment of residues 152−159 between the two protein forms results is a radically different hydrogen bonding arrangement (Table 4). The hydrogen bonding of the segment in PchF^{C} is characterized by a large number of external hydrogen bonds and one internal amide (Ala159) to carbonyl (Ser156) hydrogen bond (Figure 7). There are six hydrogen bonds to other nearby protein main or side chain atoms, one to a flavin carbonyl oxygen (O4), and two to a non-active site acetate ion. However, there is no hydrogen bond to the Gly374−Phe381 segment, the closest contact (3.2 Å) being between two nonprotonated carbonyl oxygen atoms. Three water molecules also form hydrogen bonds to the segment, one of them with main chain atoms at Phe152 and another to the carbonyl of Ile158. The third water molecule plays a central role in the hydrogen bonding arrangement of the segment. It forms hydrogen bonds with the carbonyl of Ser153 and the carbonyl and amide groups of Ser156. It is also in close nonbonded

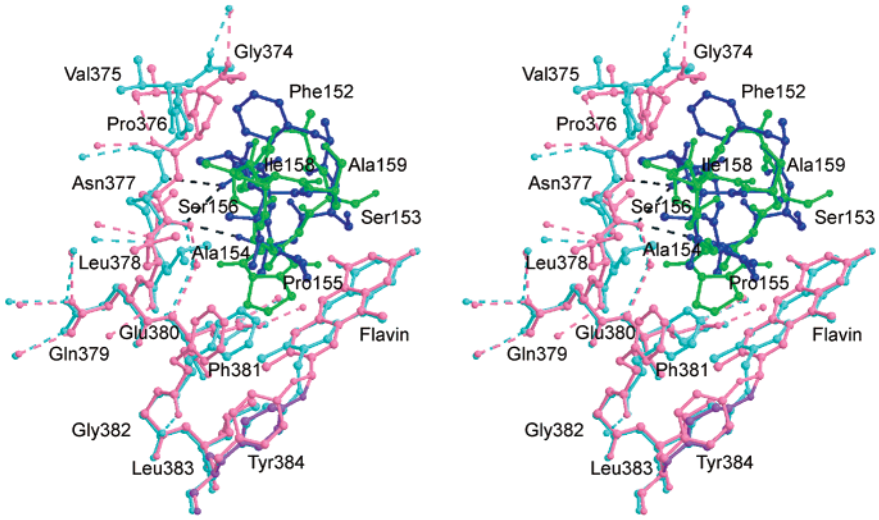

FIGURE 6: Structural comparison of the structurally aligned polypeptide segments that undergo coupled conformational changes resulting in large structural differences. The coloring scheme is the same as in Figure 5b, with the segments of residues 152−159 of rPCMH and PchF^C colored dark blue and green, respectively, and the segment of residues 374−381 (plus residues 382−384 and the covalently bound flavin ring) colored cyan and pink, respectively. The alternate conformer for Tyr384 in PchF^C is colored purple. The three hydrogen bonds between the two segments in rPCMH (Ala154 O with Asn377 O, Ser156 O$^\gamma$ with Asn377 O, and Ser156 O$^\gamma$ with Asn377 N) are shown as black dashed lines; the well-conserved set of water molecules that are bound to main and side chain atoms of the segment of residues 374−381 in the two proteins are also shown. This figure was prepared using MOLSCRIPT (*28*) and rendered with RASTER3D (*29*).

contact with the carbonyl of Ala154 (3.0 Å) and with Cβ of Ala159 (3.1 Å), the former being poorly oriented for hydrogen bond formation. The strain of these two close nonbonding contacts may be mitigated by its three strong hydrogen bonds to main chain atoms.

In rPCMH, on the other hand, there are fewer external hydrogen bonds in the segment of residues 152−159 and they are somewhat different from those in PchF^C (Figure 7). There are five internal hydrogen bonds, one in common with PchF^C. There are also five external hydrogen bonds, three to Asn377 of the Gly374−Phe381 segment, which are absent from PchF^C, and two others near the C-terminal end of the segment that are common to PchF^C. There is one hydrogen bond to a hydroxyl of the ribityl chain of FAD and one to the cytochrome subunit (Ile158 O−βTyr57 O$^\eta$). In addition, two water molecules are hydrogen bonded, one to the N and O atoms of Phe152 and one to the carbonyl oxygen of Ala157.

DISCUSSION

A key point gleaned from this structural study is that the mobile segment of residues 151−159 is strongly affected by the tight binding of PchC in the subunit interface of rPCMH. It was observed previously in the room-temperature study of PCMH and its substrate-bound complex that a portion of this segment was able to change its conformation somewhat when the substrate bound in the active site, resulting in new flavin−protein contacts (*8*). In this study, an even larger change has been observed.

The interactions between the flavoprotein and the cytochrome are strong enough (K_D = 7 nM) to induce small rearrangement of several PchF^C residues in the interface, and the effect of these small movements is transmitted back along the main chain from Ile158 within the interface to the portion of the segment directly in contact with the flavin ring. As a result, the environmental changes induced by the binding of PchC to PchF^C lead to optimization of the catalytic activity in the fully formed flavocytochrome. To wit, the mutual binding of the subunits modifies the redox potentials of the heme, FAD, and bound substrate in directions that result in significant improvement of the efficiency of substrate oxidation and electron transfers between the cofactors (see the introductory section).

One would think that the structural changes in the immediate environment around the flavin ring might influence the redox properties of the cofactor by tuning it to potentials that are appropriate for the catalytic activities of *p*-cresol hydroxylation. However, the change in potential observed for FAD from approximately 65 mV for PchF^C to approximately 85 mV for rPCMH (*13*) is not enough to account for the difference in rates for *p*-cresol oxidation by these two proteins. Recent studies by Efimov and McIntire (*10*, *18*) indicate that there is a 380 mV change in the redox potential of the bound *p*-cresol when PchC binds to PchF^C. Hence, most of the effect on the rate constant for substrate oxidation is due to a change in the potential of the bound substrate and not the FAD. Inspection of the arrangement of the isoalloxazine ring, the bound acetate, and main chain and side chain atoms of the substrate-binding domain on the *si* side offers little insight into this phenomenon since the relative disposition of these elements is nearly identical for PchF^C and rPCMH. Perhaps the structural changes next to the *re* face transmit subtle alterations in the active site environment that have a larger effect on the electronic properties of bound *p*-cresol than on those of FAD. Alternatively, the effect may be more global in origin; along with the close-range structural changes, longer-range effects, perhaps contributed by PchC (e.g., electrostatic field effects), contribute also to modulation of the electronic properties of the substrate and flavin prosthetic group.

The fact that acetate binds at the active site of PCMH in a manner resembling that of *p*-cresol suggests that the substrate is bound also in an anionic form. The phenolate form of *p*-cresol may be essential for catalysis; if the negative

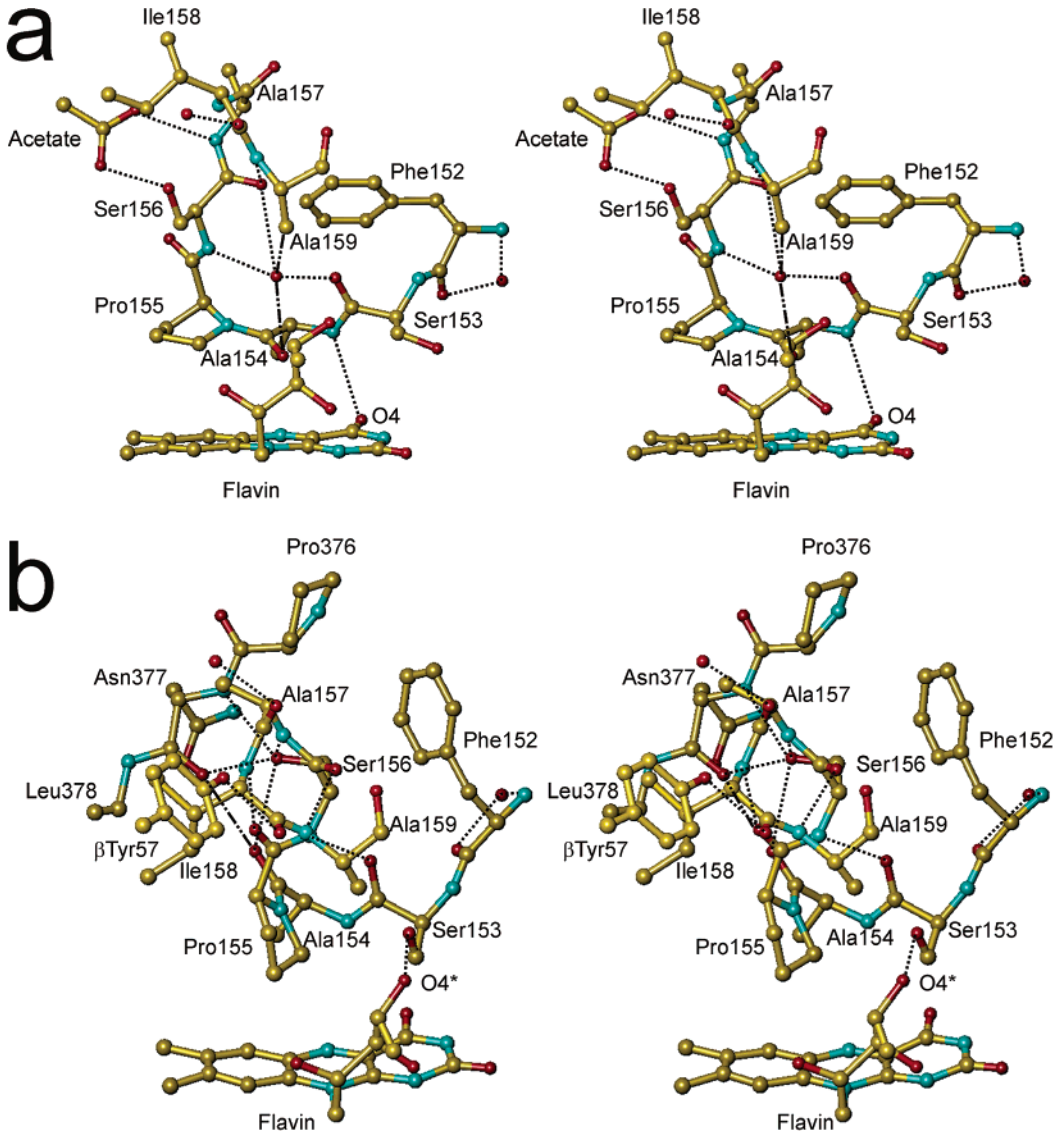

FIGURE 7: Structures of the Phe152−Ala159 polypeptide segment in PchF^C and rPCMH. (a) Polypeptide segment in atom colors of Phe152−Ala159 in PchF^C and some of its interactions with other groups. Hydrogen bonding interactions are shown as dotted lines, and two close nonbonded interactions are shown as a dashed and dotted line. The one intrasegment interaction and the interactions with three water molecules, the flavin ring, and one acetate anion are also shown. (b) Polypeptide segment in atom colors for Phe152−Ala159 in rPCMH and some of its interactions with other groups. Hydrogen bonding interactions are shown as dotted lines, and one close nonbonded interaction is shown as a dashed and dotted line. All intrasegment interactions and the interactions with Asn377, two water molecules, the flavin ribityl chain, and the side chain of βTyr57 are shown. This figure was prepared using TURBO-FRODO (*30*).

charge localized at the phenolate oxygen is destabilized (via electrostatic or hydrophobic forces), electron density at this site would be delocalized into the toluene portion of the substrate. This would result in a weakening of the methyl C−H bond of the substrate, which would facilitate hydride transfer to FAD.

It was found that the phenyl ring of Tyr384 in PchF^C can assume two conformations. Apparently, when PchC binds to the flavoprotein, the phenyl ring locks into the most favorable position for catalysis and electron transfer between the prosthetic groups. Since acetate binds in a manner similar to that of *p*-cresol in PCMH (*8*) (Figure 3), we suspect that acetate mimics also substrate binding in PchF^C (Figure 4). Hence, *p*-cresol binding may not affect dramatically the equilibrium between the two conformations of Tyr384. It is possible that equilibrium between the conformations causes fluctuations in the orientation of the flavin's isoalloxazine ring relative to the phenolate portion of bound *p*-cresol in the charge transfer complex, and/or alterations in other regions of or close to the active site. This may contribute to the change in the redox potential of the flavin and the dramatic difference in the redox potential of the substrate when it is bound to PCMH versus PchF^C. For example, since it is thought that *p*-cresol binds as its phenolate form (*16*), then subtle alterations in hydrogen bonding interactions, the hydrophobic environment, and/or the impinging electrostatic field may affect differently its electronic properties in the PchF^C−substrate complex versus the PCMH−substrate complex (vide supra).

Out of necessity, the enzyme must have evolved so that electron transfer from flavin to heme would be a very efficient step in the catalytic process. Putative electron transfer pathways have been calculated on the basis of the native PCMH structure (*8*), and several residues were proposed as likely participants. It is interesting to note in this study that some of those residues are found in different

Table 4: Hydrogen Bonding and Close Nonbonded Contacts Made by the Phe152−Ala159 Segment in rPCMH and PchF

atom 1	atom 2	distance (Å)	comment
PchF			
Phe152 N	Wat52	2.86	
Phe152 O	Wat52	2.73	
Ser153 OG	Asn164 ND2	2.95	
Ser153 OG	Val170 O	2.82	
Ser153 OG	His178 NE2	3.87	alternate conformation for His178
Ser153 O	Wat222	2.78	
Ala154 N	FAD O4F	3.05	
Ala154 O	Wat222	3.01	close nonbonded contact (bad angle)
Pro155 O	Asn377 O	3.20	intermediate nonbonded contact
Ser156 N	Wat222	2.95	
Ser156 OG	Arg91 NE	3.21	
Ser156 OG	acetate (#2) O	2.57	
Ser156 O	Ala159 N	3.32	internal H-bond
Ser156 O	Wat222	3.09	
Ala157 N	acetate (#2) OXT	2.87	
Ala157 O	Gly135 N	2.91	
Ile158 O	Wat214	2.73	
Ala159 Cα	Wat222	3.06	close nonbonded contact
Ala159 O	Phe134 N	2.90	
rPCMH			
Phe152 N	Wat198, 73 in subunits 1 and 2	3.00, 3.05	Wat52 in PchF
Phe152 O	Wat198, 73 in subunits 1 and 2	2.82, 2.82	Wat52 in PchF
Ser153 OG	FAD O4*	3.09, 2.99	
Ser153 O	Ser156 N	2.79, 2.78	
Ala154 O	Ser156 OG	2.98, 2.95	
Ala154 O	Asn377 O	2.93, 2.93	
Pro155 O	Ile158 N	2.95, 2.95	
Ser156 OG	Asn377 O	2.91, 2.93	
Ser156 OG	Ala157 N	2.75, 2.73	
Ser156 OG	Asn377 N	3.13, 3.20	
Ser156 O	Ala159 N	2.98, 3.01	
Ala157 O	Gly135 N	3.11, 3.10	
Ala157 O	Wat682, 815 in subunits 1 and 2	2.86, 2.94	
Ile158 O	Tyr657 OH	2.71, 2.65	
Ala159 O	Phe134 N	2.85, 2.91	

locations in the cytochrome-free structure, viz., Phe381, Pro155, and Leu378. It might be concluded that the binding of the cytochrome serves to align the crucial residues into orientations ideal for efficient electron transfer between the two cofactors.

It is tempting to ascribe a role to the concerted movements of the segment of residues 152−159 and the segment of residues 374−381 in the covalent flavinylation process, if such movements occur, when $PchF^{NC}$ combines with PchC. Such a large movement of the cyclic side group of Pro155 would allow the aromatic ring of Phe381 to reposition itself in PCMH such that the rotation of Tyr384 into one of its alternative conformation is prevented. A repositioned Leu378 and direct interactions with several residues of PchC would also assist in locking Phe381 and, hence, Tyr384 in place. This arrangement within the $PchF^{NC}$−PchC complex might then be required for the optimal orientation of the 8α-vinyl carbon of the putative reactive imino-quinonoid form of the flavin's isoalloxazine ring, the phenolate oxygen of Tyr384, and other catalytic groups required for covalent bond formation (*8*, *10*, *13*, *15*, *17*).

That covalently bound FAD is important for very avid binding between PchC and $PchF^{C}$ is evident when normal PCMH is compared to its Y384F mutant form, which can only bind FAD noncovalently. The K_D value for the interaction of the mutant flavoprotein and PchC is only 7 μM, which corresponds to a binding that is 3 orders of magnitude weaker than that between wild-type $PchF^{C}$ and PchC (*13*).

Currently, the structures of other forms of normal and mutant PchF are being refined. These structures should shed further light on the flavinylation process and substrate oxidation.

ACKNOWLEDGMENT

We thank the staff at the Structural Biology Center of the Advanced Photon Source for assistance during data collection.

REFERENCES

1. Hopper, D. J., and Taylor, D. G. (1975) Pathways for the degradation of *m*-cresol and *p*-cresol by *Pseudomonas putida*, *J. Bacteriol. 122*, 1−6.
2. Hopper, D. (1976) The hydroxylation of *p*-cresol and its conversion to *p*-hydroxybenzaldehyde in *Pseudomonas putida*, *Biochem. Biophys. Res. Commun. 69*, 462−468.
3. Cronin, C. N., Kim, J., Fuller, J. H., Zhang, X., and McIntire, W. S. (1999) Organization and sequences of *p*-hydroxybenzaldehyde dehydrogenase and other plasmid-encoded genes for early enzymes of the *p*-cresol degradative pathway in *Pseudomonas putida* NCIMB 9866 and 9869, *DNA Sequence 10*, 7−17.
4. McIntire, W., and Singer, T. P. (1982) Resolution of *p*-cresol methylhydroxylase into catalytically active subunits and reconstitution of the flavocytochrome, *FEBS Lett. 143*, 316−318.
5. Koerber, S. C., McIntire, W., Bohmont, C., and Singer, T. P. (1985) Resolution of the flavocytochrome *p*-cresol methylhydroxylase into subunits and reconstitution of the enzyme, *Biochemistry 24*, 5276−5280.
6. McIntire, W., Singer, T. P., Smith, A. J., and Mathews, F. S. (1986) Amino acid and sequence analysis of the cytochrome and flavoprotein subunits of *p*-cresol methylhydroxylase, *Biochemistry 25*, 5975−5981.
7. McIntire, W., Edmondson, D. E., Hopper, D. J., and Singer, T. P. (1981) 8α-(O-Tyrosyl)flavin adenine dinucleotide, the prosthetic group of bacterial *p*-cresol methylhydroxylase, *Biochemistry 20*, 3068−3075.
8. Cunane, L. M., Chen, Z. W., Shamala, N., Mathews, F. S., Cronin, C. N., and McIntire, W. S. (2000) Structures of the flavocytochrome *p*-cresol methylhydroxylase and its enzyme−substrate complex: Gated substrate entry and proton relays support the proposed catalytic mechanism, *J. Mol. Biol. 295*, 357−374.
9. Kim, J., Fuller, J. H., Cecchini, G., and McIntire, W. S. (1994) Cloning, sequencing, and expression of the structural genes for the cytochrome and flavoprotein subunits of *p*-cresol methylhydroxylase from two strains of *Pseudomonas putida*, *J. Bacteriol. 176*, 6349−6361.
10. Efimov, I., and McIntire, W. S. (2004) A study of the spectral and redox properties and covalent flavinylation of the flavoprotein component of *p*-cresol methylhydroxylase reconstituted with FAD analogues, *Biochemistry 43*, 10532−10546.
11. McIntire, W. S., Hopper, D. J., and Singer, T. P. (1987) Steady-state and stopped-flow kinetic measurements of the primary deuterium isotope effect in the reaction catalyzed by *p*-cresol methylhydroxylase, *Biochemistry 26*, 4107−4117.
12. Hopper, D. J. (1983) Redox potential of the cytochrome *c* in the flavocytochrome *p*-cresol methylhydroxylase, *FEBS Lett. 161*, 100−102.
13. Efimov, I., Cronin, C. N., and McIntire, W. S. (2001) Effects of noncovalent and covalent FAD binding on the redox and catalytic properties of *p*-cresol methylhydroxylase, *Biochemistry 40*, 2155−2166.
14. Mewies, M., McIntire, W. S., and Scrutton, N. S. (1998) Covalent attachment of flavin adenine dinucleotide (FAD) and flavin mononucleotide (FMN) to enzymes: The current state of affairs, *Protein Sci. 7*, 7−20.

15. Kim, J., Fuller, J. H., Kuusk, V., Cunane, L., Chen, Z. W., Mathews, F. S., and McIntire, W. S. (1995) The cytochrome subunit is necessary for covalent FAD attachment to the flavoprotein subunit of *p*-cresol methylhydroxylase, *J. Biol. Chem. 270*, 31202−31209.
16. Engst, S., Kuusk, V., Efimov, I., Cronin, C. N., and McIntire, W. S. (1999) Properties of *p*-cresol methylhydroxylase flavoprotein overproduced by *Escherichia coli*, *Biochemistry 38*, 16620−16628.
17. Efimov, I., Cronin, C. N., Bergmann, D. J., Kuusk, V., and McIntire, W. S. (2004) Insight into covalent flavinylation and catalysis from redox, spectral, and kinetic analyses of the R474K mutant of the flavoprotein subunit of *p*-cresol methylhydroxylase, *Biochemistry 43*, 6138−6148.
18. Efimov, I., and McIntire, W. S. (2005) The relationship between charge-transfer interactions, redox potentials and catalysis for different forms of the flavoprotein component of *p*-cresol methylhydroxylase, *J. Am. Chem. Soc. 127*, 732−741.
19. Singer, T. P., and McIntire, W. S. (1984) Covalent attachment of flavin to flavoproteins: Occurrence, assay, and synthesis, *Methods Enzymol. 106*, 369−378.
20. McPherson, A. (1999) *Crystallization of biological macromolecules*, Cold Spring Harbor Laboratory Press, Plainview, NY.
21. Otwinowski, Z., and Minor, W. (1997) Processing of X-ray diffraction data collected by oscillation methods, *Methods Enzymol. 276*, 307−326.
22. Navaza, J. (1994) Amore: An automated package for molecular replacement, *Acta Crystallogr. A50*, 157−163.
23. Brünger, A. T., Adams, P. D., Clore, G. M., DeLano, W. L., Gros, P., Grosse-Kunstleve, R. W., Jiang, J. S., Kuszewski, J., Nilges, M., Pannu, N. S., Read, R. J., Rice, L. M., Simonson, T., and Warren, G. L. (1998) Crystallography & NMR System: A new software suite for macromolecular structure determination, *Acta Crystallogr. D54*, 905−921.
24. Brünger, A. T. (1992) Free R-value: A novel statistical quantity for assessing the accuracy of crystal structures, *Nature 355*, 472−475.
25. Roussel, A., and Cambillau, C. (1989) in *Silicon graphics geometry partners directory*, pp 77−78, Silicon Graphics, Mountain View, CA.
26. Ramakrishnan, C., and Ramachandran, G. N. (1965) Stereochemical criteria for polypeptide and protein chain conformations. II. Allowed conformations for a pair of peptide units, *Biophys. J. 5*, 909−933.
27. Laskowski, R., Thornton, J., Moss, D., and MacArthur, M. (1993) Procheck: A program to check the stereochemical quality of protein structures, *J. Appl. Crystallogr. 26*, 283−291.
28. Kraulis, P. J. (1991) Molscript: A program to produce both detailed and schematic plots of protein structures, *J. Appl. Crystallogr. 24*, 946−950.
29. Merritt, E. A., and Bacon, D. J. (1997) Raster 3d: Photorealistic molecular graphics, *Methods Enzymol. 277*, 505−524.
30. Roussel, A., and Cambillau, C. (1991) in *Silicon graphics geometry partners directory 86*, Silicon Graphics, Mountain View, CA.

BI048020R